

Supporting Information

Effect of the Interfacial Protective Layer on $\text{NaFe}_{0.5}\text{Ni}_{0.5}\text{O}_2$ Cathode for Rechargeable Sodium-Ion Batteries

Iqra Moez^{a, b}, Dieky Susanto^{a, b}, Ghulam Ali^{a, c}, Hun-Gi Jung^{a, b},

Hee-Dae Lim^{*a, b}, Kyung Yoon Chung^{*a, b}

^a Center for Energy Storage Research, Korea Institute of Science and Technology, Hwarang-ro 14-gil 5, Seongbuk-gu, Seoul 02792, Republic of Korea

^b Division of Energy and Environment Technology, KIST School, Korea University of Science and Technology, Seoul 02792, Republic of Korea

^c U.S.-Pakistan Center for Advanced Studies in Energy (USPCAS-E), National University of Science and Technology (NUST), H-12, Islamabad, 44000, Pakistan.

Corresponding Authors

*E-mail: hdlim@kist.re.kr (H.-D.L.).

*E-mail: kychung@kist.re.kr (K.Y.C.).

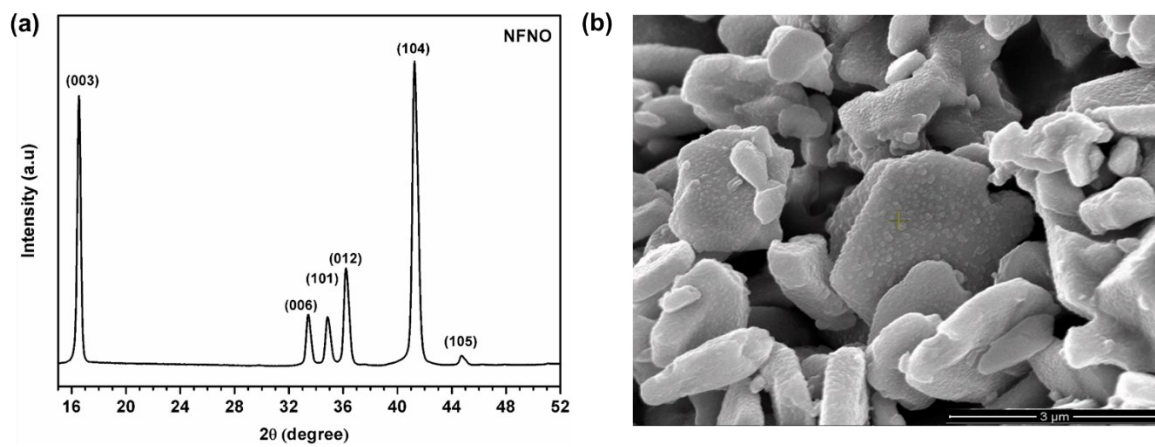


Figure S1. O₃-NaFe_{0.5}Ni_{0.5}O₂ (NFNO) structure characterizations. (a) XRD pattern and (b) SEM image of the synthesized NaFe_{0.5}Ni_{0.5}O₂ cathode material.

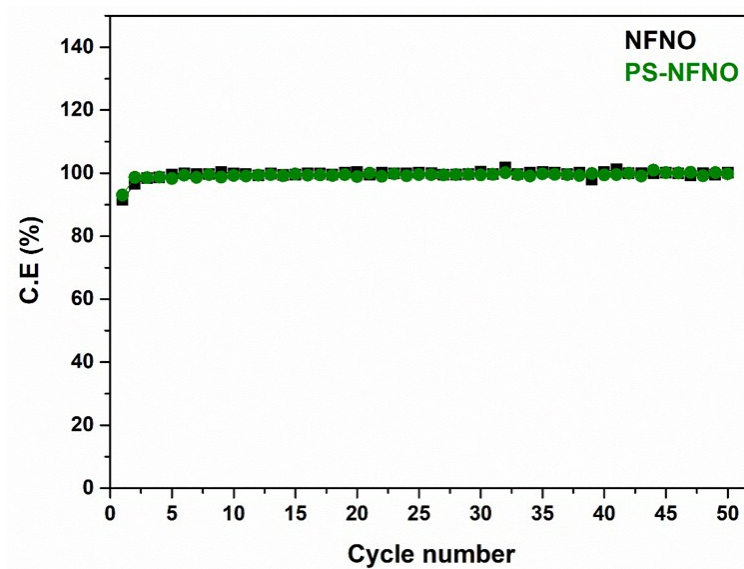


Figure S2. Comparison of the coulombic efficiency of NFNO and PS-NFNO in half-cells before and after formation of ACEI layer.

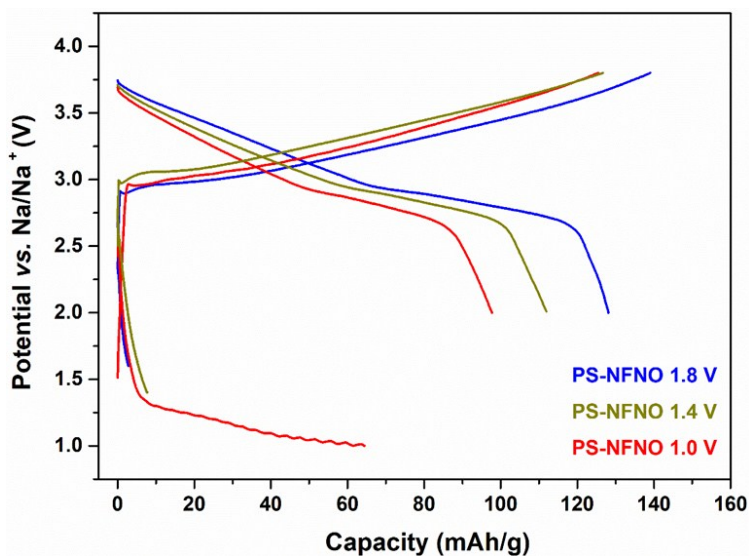


Figure S3. Voltage profile of $\text{NaFe}_{0.5}\text{Ni}_{0.5}\text{O}_2$ (NFNO) during pre-discharge process up to 1.0, 1.4, and 1.8 V SOD.

Voltage profiles for PS-NFNO, pre-discharged to 1.0, 1.4, 1.8 V demonstrate that a gradual increase in depth of pre-discharge could result in the decreases of charge and discharge capacities. The results suggest that along with the formation of thicker CEI layer, intercalation of excess sodium ions into the structure could cause a destruction of NFNO lattice by overlying excessive sodium ions between MO_x layers. Thus, it is concluded that electrochemical performance is dependent upon the structure properties, and even a slight change in crystal structure could affect the electrochemical properties of Ni based electrode material.

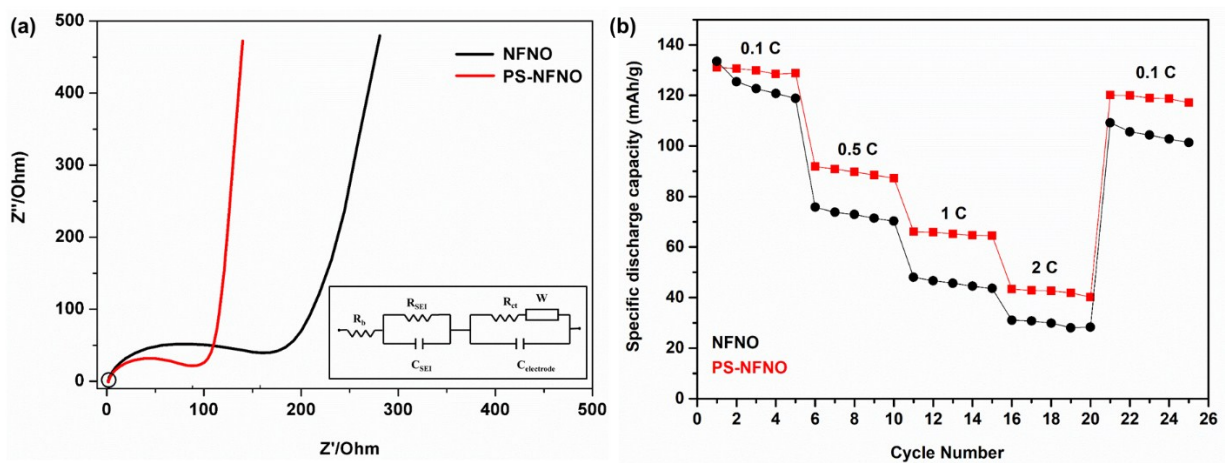


Figure S4. Electrochemical performance of $\text{NaFe}_{0.5}\text{Ni}_{0.5}\text{O}_2$. (a) Electrochemical impedance spectra (EIS) of $\text{NaFe}_{0.5}\text{Ni}_{0.5}\text{O}_2$ before and after pre-sodiation up to 1.6 V, shows reduction in the charge transfer resistance. Inset shows the equivalent circuit model for the Nyquist plot, where R_b : bulk resistance of the cell (electrolyte, separator, and electrodes), R_{SEI} and C_{SEI} : resistance and capacitance of the interphase, R_{ct} and $C_{\text{electrode}}$ demonstrate charge-transfer resistance and double layer capacitance, and W : Warburg impedance. (b) Comparison of cyclic performance of NFNO and PS-NFNO with SOD of 1.6 V at different C-rate of 0.1, 0.5, 1.0, 2.0, and 0.1 C.

Figure S4 exhibit the comparison of the nyquist plot of NFNO and PS-NFNO. EIS analysis confirmed that R_{ct} get improved after formation of ACEI layer on PS-NFNO. Na_2CO_3 , NaF , Na_2O , carbonaceous and oxygenated species formed a thicker ACEI layer on the surface of PS-NFNO that could provide fast and reversible intercalation/de-intercalation of sodium ions and reduce the charge transfer resistance. Hence, the estimated and controlled content of these species in ACEI could effectively enhance the kinetics of the battery.

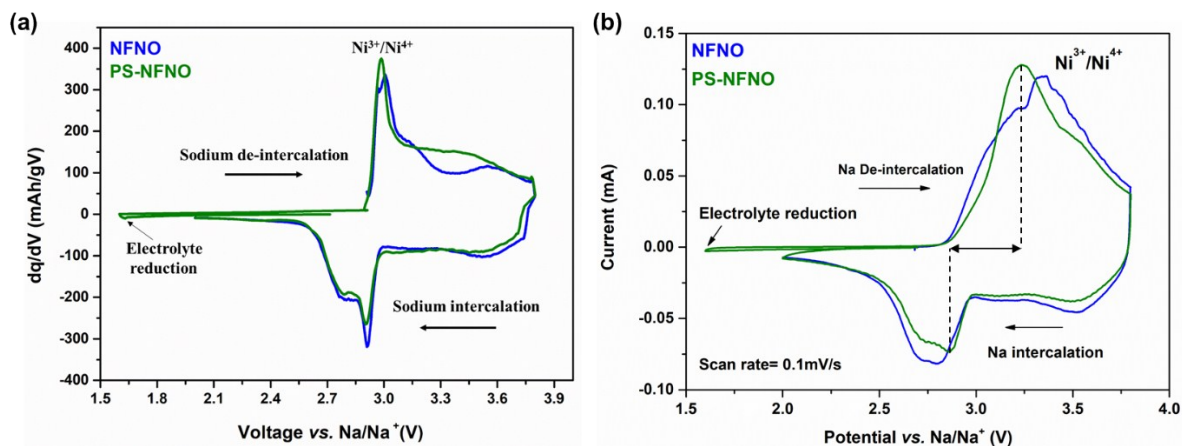


Figure S5. Electrochemical performance of NFNO and PS-NFNO. (a) Differential capacity curves (b) cyclic voltammetry (CV) curves corresponding to the first cycle plotted with respect to voltage for the half-cell of NFNO and PS-NFNO.

Differential and cyclic voltammetry curves for both NFNO and PS-NFNO electrodes (Fig. S5a and b) exhibit a pair of redox peaks which correspond to Ni³⁺/Ni⁴⁺ redox reaction and well matched with the previous report¹. A small reduction peak for PS-NFNO at 1.6 V vs. Na/Na⁺ in differential and CV curves corresponds to electrolyte reduction and formation of ACEI layer during pre-discharge process. PS-NFNO CV curve clearly demonstrate that after formation of ACEI layer, structure stability and its reversibility get improved, leading to the excellent capacity retention of Ni-based cathode material for NIBs.

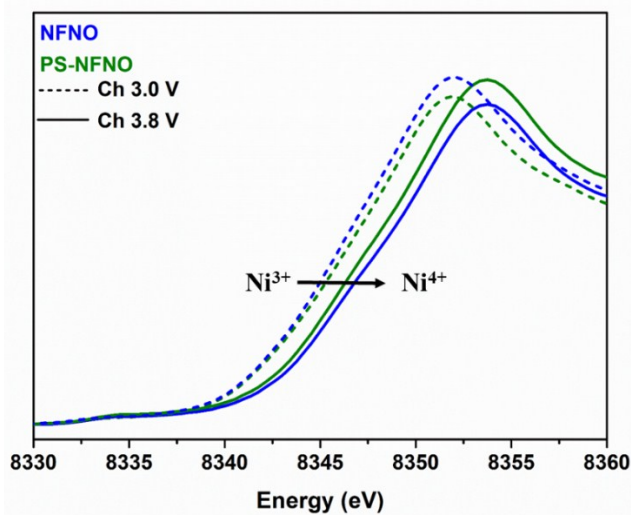


Figure S6. Characterization of NFNO electrodes by XAS spectroscopy. XANES spectra of NFNO and PS-NFNO at Ni K-edges during charge process at cut-off voltages of 3.0, and 3.8 V.

Figure S6 shows the comparisons for the Ni valence oxidation states of NFNO and PS-NFNO during charge process. XAS spectra for PS-NFNO exhibits that the average oxidation of Ni is less than that of NFNO. It might be due to reduction in Ni redox activity during charge process. It is suggested that after pre-sodiation process, existence of excess sodium ions in the PS-NFNO could be reason of this reduction. Similar trends were also observed for Ni based NMC (nickel, manganese and cobalt) cathode material for lithium-ion batteries (LIBs) ^{2,3}, which confirmed that Ni redox activity is highly dependent upon the structure properties. Hence, a slight change in structure properties could affect the electrochemical reactions of these electrode materials.

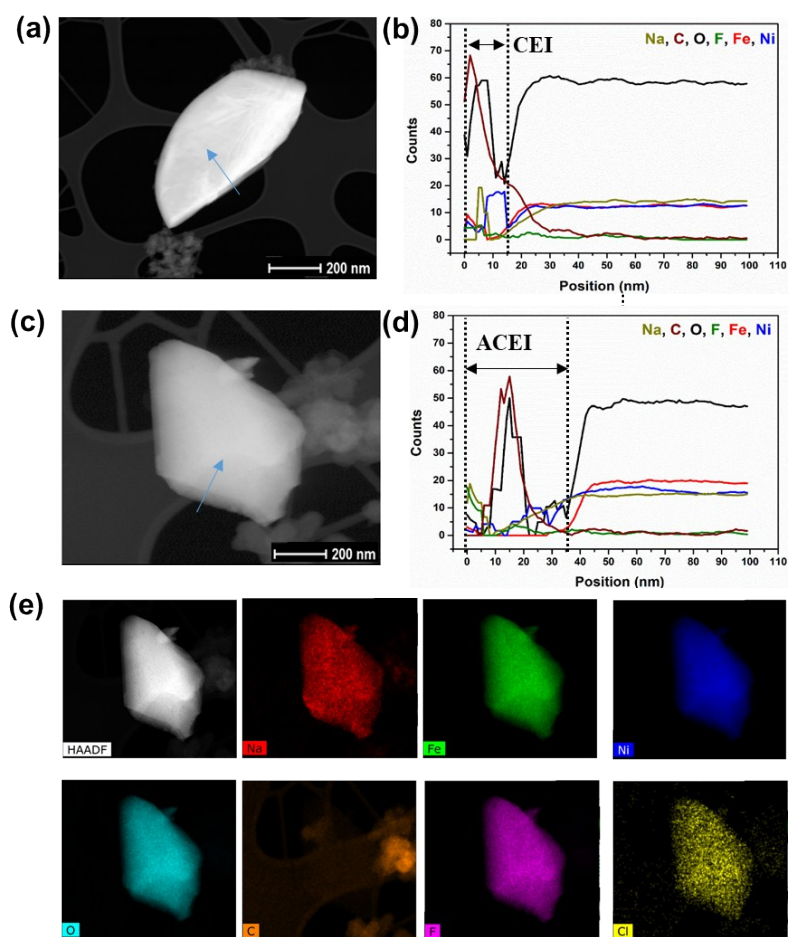


Figure S7. TEM–EDS line scanning images of (a, b) NFNO and (c, d) PS-NFNO showing formation of thick ACEI layer after pre-sodiation process. (e) TEM-EDS element mapping of PS-NFNO 1.6 V.

Fig. S7 shows elemental concentration profiles by EDS line scan across the interface which was conducted to obtain the compositional information CEI layer for NFNO before and after pre-sodiation. Na, C, and F (Fig. S7 a, b) are selected for the elements defining CEI region while Fe is chosen for representing NFNO region. EDS line profile of Ni and O elements exhibit co-existence of them, inside and at the surface of NFNO particle^{2,4,5}. Hence Fe profile is chosen to a criterion

to determine the thickness of the CEI layer. During pre-sodiation (Fig. S7 c, d.), the concentration of Na, O, C, and F is increased due to reduction of electrolyte and its additive. In addition, the overall element mapping proved the existences of Na, Fe, Ni, O, C, F, and Cl elements in the electrode and ACEI layer (Fig. S7 e). Which implies that after pre-sodiation, Na, O, C, and F based species formed a thick ACEI layer on PS-NFNO. Formation of ACEI layer on PS-NFNO is estimated to be ~ 35 nm as shown in Fig. S7 c, d. The coverage of cathode surface by this thick interphase effectively prevented metal dissolution and minimized the side reactions of Ni during the subsequent cycling process^{2,3,6}.

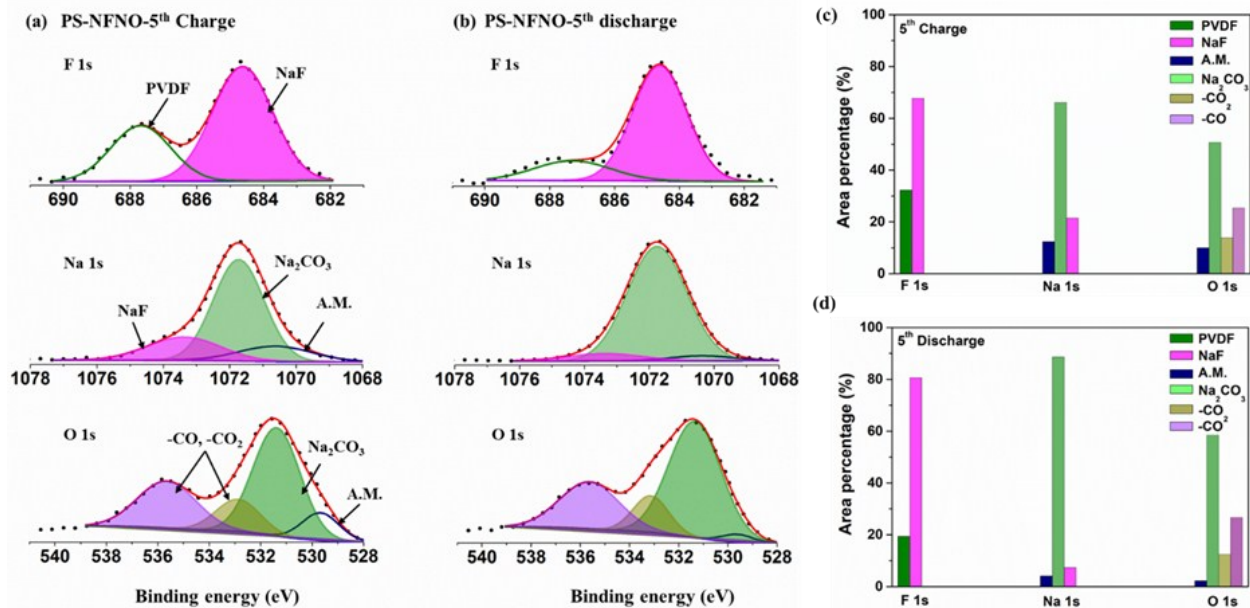


Figure S8. Dynamic evaluation of ACEI formation and dissolution. (a) Comparison of F 1s, Na 1s, and O 1s XPS spectra of PS-NFNO electrode after completion of 5th (a) charge and (b) discharge process with their (c, d) respective comparison of area percentages. Dotted (black) and solid (red) spectra represent the observed spectra and summation of peak energies, respectively.

In the XPS result of PS-NFNO after completion of 5th charge and discharge process (Fig. S8), it is confirmed that ACEI formed on the cathode surface undergoes continuous formation and decomposition during repeated charge and discharge process. During discharge process (Fig. S8b and S8d), gradual decrease in the intensity of peaks associated to PVDF binder in F 1s spectra and active material (A.M.) in Na 1s and O 1s spectra, compared to NaF, Na₂CO₃, -CO and -CO₂ species clearly proves that electrolyte and its additive are reduced during discharge process and formed a thick ACEI layer. However, these species are not stable at high voltages and partially

decompose during charge process (Fig. S8a and S8c). Furthermore, the comparison of percentage of peak areas clearly demonstrate that concentration of NaF, Na₂CO₃, and carbonaceous and oxygenated species (-CO, -CO₂) get increased during discharge process and gradually decrease with the voltage during charge process. This dynamic evaluation behavior of ACEI in initial cycles highlight a correlation of cathode-electrolyte interphase and its surface composition with the potential.

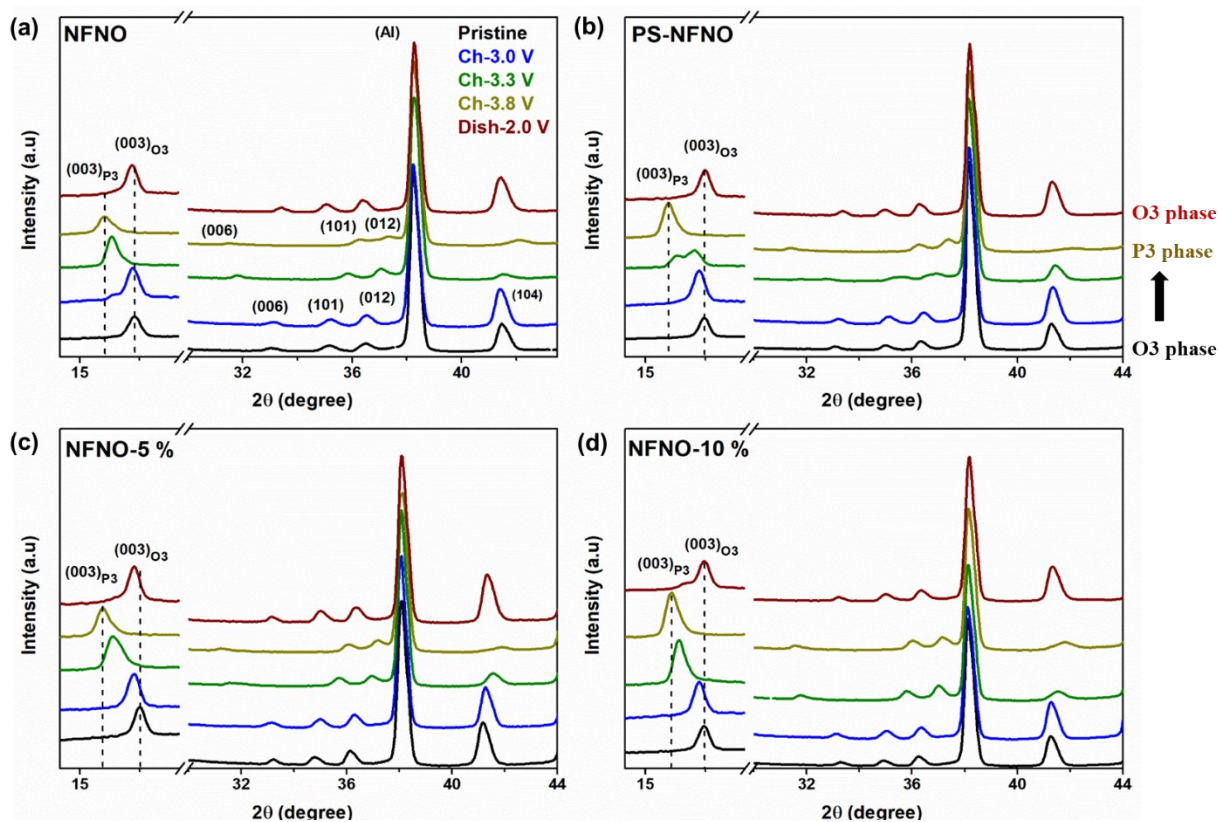


Figure S9. Comparison of *ex-situ* XRD patterns of (a) NFNO, (b) PS-NFNO, (c) NFNO-5 %, and (d) NFNO-10 % showing reversible O3 to P3 phase transition during charge and discharge process.

Fig. S9 presents the comparison of *ex-situ* XRD patterns of NFNO, PS-NFNO, NFNO-5%, and NFNO-10% during cycling process. After a charge to 3.3 V, all the electrodes, except for PS-NFNO, showed transition from O3 to P3 phase¹. The *ex-situ* XRD patterns for the fully charged state at the potential of 3.8 V confirmed a complete P3 phase formation for the all electrode materials. For the fully discharged electrodes (at 2.0 V), NFNO, NFNO-5 % and NFNO-10 % showed a biphasic behavior (O3 and P3) compared to their respective pristine electrodes. This incomplete phase transition could be due to intercalation of solvent molecules and/or salts ions

into the structure at sodium vacant sites, during charge process ⁷. Formation of metal fluoride (*e.g.* NiF and MnF) under the attack of electrolyte and its decomposition is the origin of barrier for Na⁺ diffusion into the structure. However, complete passivation of PS-NFNO surface with ACEI layer during charge process can protect the electrode material from these electrolyte attack and enhance the electrochemical performance of the cathode material.

Table S1. Lattice parameters $\text{NaFe}_{0.5}\text{Ni}_{0.5}\text{O}_2$ and with excess of sodium ions.

Electrode	a=b (Å^0)	c (Å^0)
NFNO	2.9649	16.2873
NFNO-1.6V	2.9690	16.2703
NFNO-5%	2.9710	16.0880
NFNO-10%	2.9763	15.9965

References

1. Nanba, T. Iwao, B. M. DeBoisse, W. Zhao, E. Hosono, D. Asakura, H. Niwa, H. Kiuchi, J. Miyawaki, Y. Harada, M. Okubo and A. Yamada, *Chem. Mater.*, 2016, **28**, 4.
2. Z. Wu, S. Ji, Z. Hu, J. Zheng, S. Xiao, Y. Lin, K. Xu, K. Amine and F. Pan, *ACS Appl. Mater. Interfaces*, 2016, **8**, 24.
3. Z. Wu, S. Ji, J. Zheng, Z. Hu, S. Xiao, Y. Wei, Z. Zhuo, Y. Lin, W. Yang, K. Xu, K. Amine, F. Pan, *Nano Lett.*, 2015, **15**, 5590–5596.
4. J. H. Woo, J. E. Trevey, A. S. Cavanagh, Y. S. Choi, S. C. Kim, S. M. George, K. H. Oh and S. H. Lee, *J. Electrochem. Soc.*, 2012, **7**, A1120–A1124.
5. Z. Zeng, X. Zhang, K. Bustillo, K. Niu, C. Gammer, J. Xu and H. Zheng, *Nano Lett.*, 2015, **15**, 5214–5220.
6. T. Kim, L. K. Ono, N. Fleck, S. R. Raga and Y. Qi, *J. Mater. Chem. A*, 2018, **6**, 14449–14463.
7. S. Komaba, C. Takei, T. Nakayama, A. Ogata and N. Yabuuchi, *Electrochem. Commun.*, 2010, **12**, 355–358.